RESEARCH ARTICLE

Viscosity of evolving magmas: a case study of the Glass House Mountains, Australia

Sharon L. Webb[1]

Abstract

The viscosity of the remelted rock compositions of the Glass House Mountains, SE Queensland, Australia, has been determined via micro-penetration in the high-viscosity regime (10^8–10^{13} Pa s). The heat capacity of these melts has also been determined from room temperature to above the glass transition. The combination of these two data sets allows the fitting of the viscosity data by the Adam-Gibbs equation using the configurational heat capacity $C_p^{conf}(T_g^{12})$ and configurational entropy $S_{conf}(T_g^{12})$. The resulting fit parameters allow the robust extrapolation of the viscosity data to higher temperature and viscosities of 10^{-4} Pa s. This data can now be used in the discussion of the emplacement of the magmas of the plugs, laccoliths, sills and dykes that form the Glass House Mountains complex and the plate motion and the plume responsible for the volcano plugs. The large increase in viscosity of the evolving magma and the resulting decrease in discharge rate of the volcanic vents suggest that very little magma appeared as extrusive lavas or pyroclastic material and that the Glass House Mountains are mainly remnants of intrusive bodies exposed by erosion.

Keywords Glass House Mountains · Viscosity · Heat capacity · Entropy

Introduction

There is a growing interest in the 9–33 million years old plume track across Eastern Australia from Cape Hillsborough (QLD) to Cosgrove (Vic) (Cohen et al. 2013; Davies et al. 2015). The Noosa-Maleny-Glass House Mountains complex (hereafter called GHM) is a small suite of volcanoes in SE Queensland that is associated with this plume track (see Fig. 1). The GHM volcanoes have been dated in the Oligocene at 26 million years (Cohen et al. 2007). The shape of these plugs is similar to that of glass furnaces in Great Britain, hence the name given to them by Cook in 1770. Recent analysis of major and trace elements of rocks from the Glass House Mountains as well as Sr, Nd and Pb isotopic data by Shao et al. (2015) has shown the GHM volcanoes to be the product of an evolving magma chamber with the magma compositions progressing from basaltic lava flows in the Maleny region, to the Glass House Mountains volcanic plugs whose composition ranges from basaltic, basaltic trachy-andesite to trachyandesite, trachyte and peralkaline rhyolite of comendite composition (see Fig. 2). The peraluminous rhyolite of Mt Tinbeerwah in the Noosa area is assumed to be formed by basaltic underplating causing crustal anatexis.

Although the composition and mineralogy of the volcanic plugs in the Glass House Mountains series are now known and they are assumed to be related through fractional crystallisation, little else is known of the flow and emplacement mechanisms of the magmas responsible for these volcanoes. Except for an early study (Bryan and Stevens 1973) there is no information of the emplacement temperatures of the magmas.

The viscosity of magmas of basaltic, andesitic and rhyolitic compositions have been determined (e.g. Vetere et al. 2008; Whittington et al. 2009; Di Genova et al. 2013; Webb et al. 2014; Sehlke and Whittington 2016); however, there are very few studies of the continuous change in viscosity with evolution of the magma chamber by fractional crystallisation. There is little data on the viscosity of subaluminous comenditic melts with Stevenson et al. (1995) investigating the viscosity of naturally occurring metaluminous comenditic obsidians which had not been remelted in the laboratory. Although the viscosity of magma of known
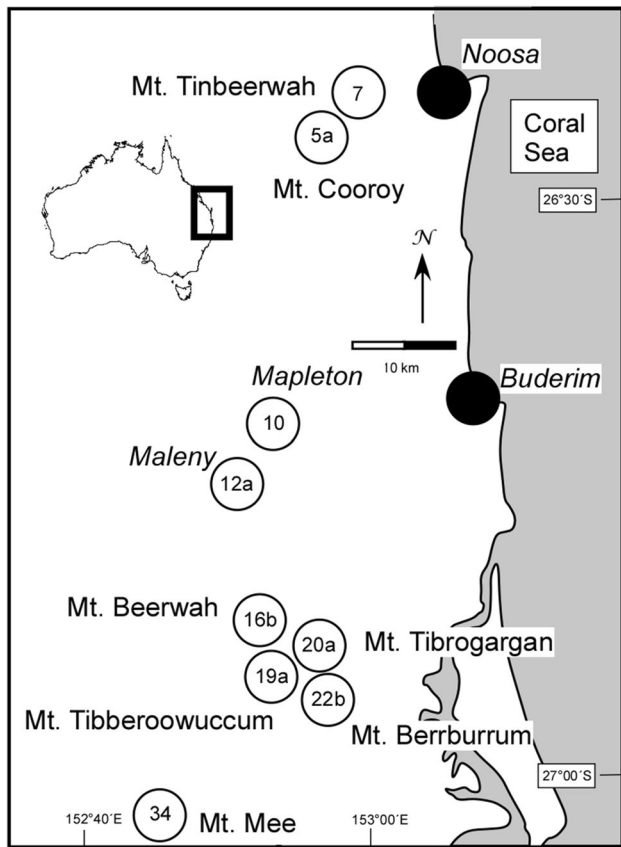

✉ Sharon L. Webb
   swebb@gwdg.de

1 Mineralogy Department, Georg-August University, GZG, Goldschmidtstr. 1, Göttingen, Germany

Fig. 1 Map of the Glass House Mountains region (after Shao et al. 2015). The locations of the sampled volcanoes are indicated. For a geological map of Cenozoic volcanic rocks of southeast Queensland see Shao et al. (2015). Location of main map on the east coast of Australia is given as inset

composition can be estimated to within ± 1.5 $\log_{10}$ units using any of a range of viscosity models (e.g. Giordano

et al. 2008; Misiti et al. 2011; Di Genova et al. 2013; Robert et al. 2015), it remains necessary to measure the viscosity of silicate melts in order to obtain accurate data.

Experiments

Sample preparation

A series of nine compositions has been chosen from the 34 rock analyses of Shao et al.'s (2015) paper on the petrogenesis of the peralkaline rhyolites of the Glass House Mountains. Melts of the compositions determined by Shao et al. (2015) were made from powders of oxides and carbonates. These powders were dried at 500 °C (1000 °C for MgO) for 12 h, weighed into a $Pt_{90}Rh_{10}$ crucible and decarbonated at 1000 °C for 12 h. The resulting material was melted at 1600 °C for 1 h, quenched to a glass, crushed in an agate mortar and remelted twice. Sample 7 (Mt. Tinbeerwah) was melted at 1625 °C. The compositions of the resulting glasses were determined by electron microprobe and are presented in Table 1. The iron speciation was determined by wet chemistry analysis after Wilson (1969) and Schuessler et al. (2008). Iron-free (haplo-)glasses were also synthesised. In these glasses, 50% of the mole fraction of FeO_{tot} was assumed to be Fe^{3+} and was therefore replaced by Al_2O_3, and the rest was replaced by MgO. MgO was chosen over CaO as the radius of Mg is closer to that of Fe than Ca radius is (Shannon and Prewitt 1969). The compositions of these glasses were also determined by electron microprobe and are given in Table 2. The polymerisation of the melts has been described in terms of γ [$\sum (X_2O + YO)/ \sum (X_2O + YO + Al_2O_3 + Fe_2O_3)$ in mol. fraction] and NBO/T (non-bridging oxygens per tetrahedron = (2O-4 T)/T, in

Fig. 2 Chemistry of the GHM melts as a function of SiO_2 content. The T_g^{12} values determined from the viscosity measurements are also plotted as is the polymerization parameter γ for each melt
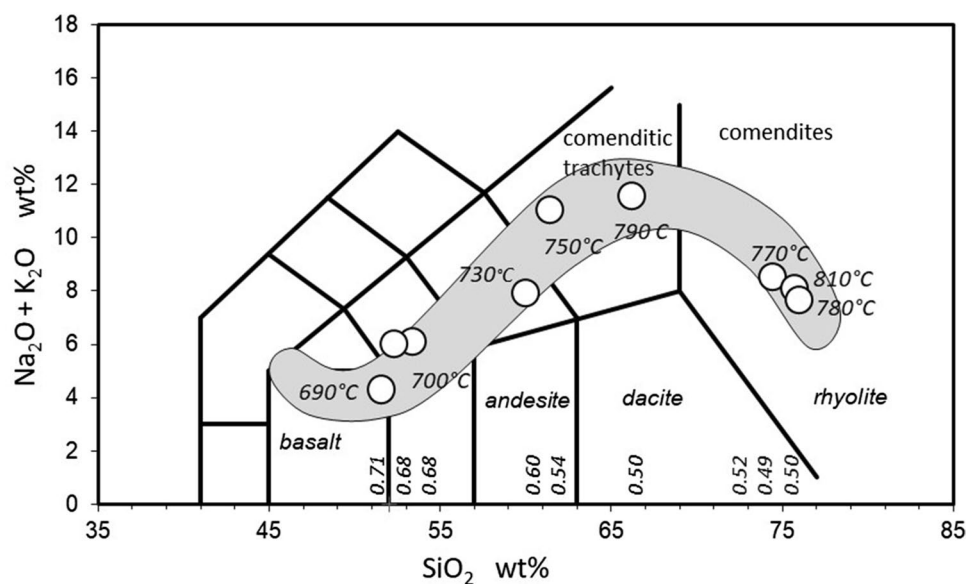
Table 1 Composition of the iron-bearing glasses determined by electron microprobe analysis (JEOL JXA 8900 RL) with 15-kV acceleration voltage, 15-nA current and 25-μm beam diameter. Listed data are the average of 10 single measurements; in both wt% and mol%.

Shao et al	20a	19a	16b	22b	5a	34	12a	10	7
Location	Mt. Tibrogargan	Mt. Tibberoowuccum	Mt. Beerwah	Mt. Beerburrum	Mt. Cooroy	Mt. Mee	Maleny	Mapelton	Mt. Tinbeerwah
wt%	Comendite	Comendite	Comenditic-trachyte	Trachyte	Syenite	Basaltic trachy-andesite	Trachy-basalt	Basalt	Peraluminous rhyolite
SiO_2	75.93 ± 1.06	74.36 ± 0.54	66.18 ± 0.32	61.11 ± 0.28	59.95 ± 0.331	52.80 ± 0.35	52.31 ± 0.26	51.72 ± 0.08	75.68 ± 0.26
Al_2O_3	12.06 ± 0.54	11.54 ± 0.36	17.60 ± 0.15	17.43 ± 0.09	15.72 ± 0.09	15.61 ± 0.09	15.38 ± 0.14	15.47 ± 0.11	$13.230 \pm .02$
TiO_2	0.27 ± 0.02	0.14 ± 0.02	0.14 ± 0.03	0.31 ± 0.02	1.38 ± 0.03	2.01 ± 0.05	2.47 ± 0.02	1.51 ± 0.03	0.08 ± 0.02
FeO	2.04 ± 0.23	3.91 ± 0.18	3.54 ± 0.07	5.73 ± 0.07	7.35 ± 0.06	10.10 ± 0.22	10.09 ± 0.04	10.73 ± 0.09	1.63 ± 0.04
MgO	–	–	0.04 ± 0.01	0.37 ± 0.02	1.60 ± 0.04	5.44 ± 0.09	4.65 ± 0.02	6.89 ± 0.07	0.23 ± 0.02
CaO	0.19 ± 0.02	0.10 ± 0.01	0.39 ± 0.02	2.09 ± 0.04	3.84 ± 0.07	5.97 ± 0.07	7.56 ± 0.02	7.70 ± 0.07	0.47 ± 0.01
Na_2O	4.73 ± 0.20	4.57 ± 0.12	6.69 ± 0.10	5.36 ± 0.11	4.75 ± 0.08	4.09 ± 0.08	4.04 ± 0.06	3.57 ± 0.05	3.20 ± 0.06
K_2O	2.84 ± 0.23	3.94 ± 0.04	4.74 ± 0.04	5.69 ± 0.06	3.38 ± 0.05	2.23 ± 0.03	1.90 ± 0.06	0.78 ± 0.03	4.74 ± 0.06
Total	98.07	98.53	99.31	98.11	98.00	98.27	98.43	98.38	99.31
Fe^{2+}/Fe^{tot}	0.472 ± 0.033	0.398 ± 0.022	0.424 ± 0.016	0.454 ± 0.021	0.474 ± 0.013	0.461 ± 0.012	0.473 ± 0.014	0.524 ± 0.023	0.557 ± 0.033
mol%	20a	19a	16b	22b	5a	34	12a	10	**7**
SiO_2	83.34 ± 0.70	82.06 ± 0.42	74.60 ± 0.28	70.47 ± 0.13	68.10 ± 0.08	58.94 ± 0.24	58.37 ± 0.13	56.66 ± 0.09	82.64 ± 0.17
Al_2O_3	7.81 ± 0.38	7.51 ± 0.22	11.69 ± 0.11	11.85 ± 0.07	10.52 ± 0.06	10.27 ± 0.05	10.11 ± 0.05	9.99 ± 0.05	8.52 ± 0.09
TiO_2	0.22 ± 0.02	0.11 ± 0.02	0.12 ± 0.03	0.27 ± 0.02	1.18 ± 0.03	1.69 ± 0.04	2.08 ± 0.04	1.24 ± 0.03	0.07 ± 0.01
FeO	0.88 ± 0.11	1.44 ± 0.10	1.42 ± 0.06	2.51 ± 0.12	3.31 ± 0.10	4.35 ± 0.15	4.46 ± 0.13	5.15 ± 0.23	0.83 ± 0.05
Fe_2O_3	0.49 ± 0.23	1.09 ± 0.19	0.96 ± 0.09	1.51 ± 0.13	1.84 ± 0.12	2.54 ± 0.27	2.48 ± 0.14	2.34 ± 0.24	0.33 ± 0.06
MgO	0.01 ± 0.02	0.01 ± 0.01	0.03 ± 0.02	0.63 ± 0.03	2.71 ± 0.08	9.06 ± 0.16	7.73 ± 0.08	11.25 ± 0.11	0.37 ± 0.03
CaO	0.22 ± 0.02	0.12 ± 0.02	0.47 ± 0.02	2.59 ± 0.05	4.67 ± 0.08	7.14 ± 0.08	9.05 ± 0.11	9.03 ± 0.07	0.55 ± 0.03
Na_2O	5.04 ± 0.23	4.89 ± 0.13	7.31 ± 0.10	5.99 ± 0.11	5.23 ± 0.08	4.43 ± 0.09	4.37 ± 0.07	3.80 ± 0.05	3.39 ± 0.06
K_2O	1.98 ± 0.04	2.77 ± 0.03	3.41 ± 0.03	4.18 ± 0.04	2.45 ± 0.04	1.59 ± 0.02	1.36 ± 0.02	0.54 ± 0.02	3.30 ± 0.04
molar mass (g mol^{-1})	64.743	65.536	67.409	68.209	67.162	66.314	66.384	65.118	65.186
γ	0.495	0.518	0.500	0.543	0.598	0.675	0.682	0.707	0.488
NBO/T	-0.003	0.013	0.000	0.052	0.128	0.319	0.336	0.422	-0.008

NBO/T = (2O-4 T)/T

$γ = (Na_2O + K_2O + FeO + MgO + CaO)/(Na_2O + K_2O + FeO + MgO + CaO + Fe_2O_3 + Al_2O_3)$ in mol. fraction

mol. fraction). Comparison of γ and NBO/T for the iron-bearing melts and their respective iron-free samples are in good agreement, except for 20a for which the iron-free haplo-melt has too many network modifying cations and is slightly metaluminous, whereas the iron-bearing melt is peraluminous. The viscosity and heat capacity of the series of iron-free melts were also determined. These melts are labelled as haplo-GHM samples.

Viscometry

The viscosity was determined in air by the micro-penetration technique in which a 2-mm diameter single crystal sphere of corundum is forced into the sample at a fixed load at a constant temperature. Newtonian, time-independent viscosity is determined by:

$$\eta = \frac{0.1875 \, F \, t}{r^{0.5} \, l^{1.5}} \tag{1}$$

for t time (s), l indent distance (m), F applied force F (N), r radius (m) of the sphere and 0.1875 a geometrical constant (Pocklington 1940; Dingwell et al. 1992). Forces from 0.2 to 5 N were used for indent times from 15 min to 12 h. Viscosities in the range 10^8–10^{13} Pa s were determined. The samples were heated to the measurement temperature at a rate of 10 K min^{-1}. The structure of the melt was allowed to equilibrate thermodynamically for 20 min before the force was applied and the indenter pushed into the melt. This amount of time was also needed for the temperature of the furnace to stabilise within ± 0.5 K. As these melts are highly viscous, some of the data were collected over a 12-h period with the unrelaxed penetration data being discarded. In general, mechanically relaxed penetration data were obtained ~ 100 τ after the application of the load, where

$$\tau = \eta_0/G_\infty \tag{2}$$

is the relaxation time calculated from the Maxwell equation (Maxwell 1867; Webb 1991) for η_0 the time independent

Table 2 Composition of the iron-free glasses determined by electron microprobe analysis (JEOL JXA 8900 RL) with 15-kV acceleration voltage, 15-nA current and 25-μm beam diameter. Listed data are the average of 10 single measurements; in both wt% and mol%

wt%	h20a	h19a	h16b	h22b	h5a	h34	h12a	h10	h7	NIQ
SiO_2	74.78±0.72	75.90±0.58	67.02±0.30	63.28±0.23	61.81±0.31	55.27±0.28	54.06±0.12	54.35±0.15	76.31±1.50	42.74±0.23
Al_2O_3	13.59±0.41	13.15±0.42	18.74±0.13	20.00±0.12	18.65±0.14	20.03±0.18	20.15±0.09	20.02±0.12	13.32±0.94	10.03±0.15
TiO_2	0.13±0.02	0.15±0.03	0.13±0.02	0.32±0.01	1.36±0.02	2.13±0.04	2.57±0.03	1.57±0.03	0.10±0.01	2.93±0.02
MgO	0.85±0.03	0.94±0.04	0.90±0.02	1.83±0.03	3.61±0.04	8.49±0.08	7.79±0.06	10.19±0.09	0.61±0.09	8.93±0.04
CaO	0.12±0.01	0.09±0.01	0.40±0.02	2.14±0.06	3.91±0.04	6.35±0.11	8.14±0.06	8.12±0.07	0.46±0.07	25.76±0.04
Na_2O	5.23±0.16	4.89±0.12	7.03±0.09	5.53±0.07	5.81±0.07	4.17±0.05	4.07±0.05	3.66±0.05	3.21±0.23	7.65±0.05
K_2O	4.15±0.09	3.94±0.07	4.78±0.05	5.93±0.09	3.43±0.04	2.33±0.04	1.94±0.03	0.82±0.03	4.78±0.15	1.06±0.07
Total	98.86	99.06	99.09	99.03	98.57	98.76	98.73	98.73	97.78	99.10
mol%	h20a	h19a	h16b	h22b	h5a	h34	h12a	h10	h7	NIQ
SiO_2	81.27±0.78	82.04±0.63	74.66±0.33	70.72±0.26	67.77±0.34	59.01±0.30	57.89±0.13	57.03±0.16	83.13±0.16	42.81±0.23
Al_2O_3	8.70±0.26	8.37±0.27	12.28±0.09	13.17±0.08	12.05±0.09	12.61±0.11	12.71±0.06	12.38±0.07	8.55±0.06	5.92±0.09
TiO_2	0.11±0.02	0.12±0.03	0.11±0.02	0.27±0.01	1.12±0.02	1.71±0.03	2.07±0.02	1.24±0.02	0.08±0.01	2.21±0.02
MgO	1.37±0.05	1.52±0.07	1.49±0.03	3.05±0.05	5.89±0.07	13.50±0.13	12.43±0.10	15.94±0.14	0.99±0.15	13.33±0.06
CaO	0.14±0.01	0.10±0.01	0.48±0.02	2.56±0.07	4.59±0.05	7.26±0.13	9.34±0.07	9.13±0.08	0.53±0.08	27.65±0.04
Na_2O	5.51±0.17	5.13±0.13	7.58±.01	5.99±0.08	6.18±0.07	4.31±0.05	4.23±0.05	3.73±0.05	3.39±0.21	7.43±0.05
K_2O	2.88±0.26	2.72±0.05	3.39±0.04	4.23±0.07	2.40±0.03	1.59±0.03	1.32±0.02	0.55±0.02	3.32±0.10	0.64±0.04
molar mass [g mol^{-1}]	64.53	64.34	66.23	66.50	64.94	63.36	63.52	62.25	64.66	59.60
γ	0.53	0.53	0.51	0.55	0.613	0.679	0.682	0.703	0.490	0.89
NBO/T	0.02	0.02	0.01	0.05	0.15	0.33	0.34	0.41	-0.01	1.52

shear viscosity and G_∞ the elastic shear modulus (Herzfeld and Litovitz 1959). The melt samples used for the viscosity measurements were ~ 3-mm-thick with an irregular shape varying from 6 to 10 mm in cross-section. The ends were ground parallel and polished with 1 μm Al_2O_3 powder before the viscosity measurements. The ± 0.06 log_{10} unit accuracy of the viscosity measurements was determined from the viscosity of DGG1 glass (Webb 2005) as well as from a further glass sample—NIQ (Whittington et al. 2000). The measured composition of the NIQ sample is given in Table 2.

Heat capacity

The heat capacity of the melts was determined using a Netzsch® DSC 404C at a heating rate of 20 K min^{-1} on samples which had first been heated to temperature above the glass transition temperature and then cooled at a rate of 20 K min^{-1}. The heat capacity is measured against an empty Pt crucible. The heat flow is calibrated at the same heating rate as the glass measurements against a single crystal of Al_2O_3 and the heat capacity data from Robie et al. (1978). The heat capacity measurements are performed at temperature between 20 °C and that at which η ~ 10^9 Pa s. The structural relaxation time at this viscosity is ~ 0.1 s and therefore holding the melt at this temperature for 60 s before controlled cooling will allow the fictive temperature of the melt to be reset to that of the 20 K min^{-1} cooling rate used in the subsequent measurements.

The configurational heat capacity $C_p^{conf}(T^*)$ (Richet 1984; Webb 2008) is calculated from an extrapolation of the Maier and Kelley (1932) equation:

$$C_p^{MK}(T) = a + bT - cT^{-2} \tag{3}$$

for heat capacity as a function of temperature $c_p(T)$ and temperature T in K, fit to the unrelaxed glass part of the heat capacity curve, and the measured relaxed liquid heat capacity

$$C_p^{conf}(T^*) = C_p^{liquid}(T^*) - C_p^{MK}(T^*). \tag{4}$$

The limiting fictive temperature of the samples is calculated using the method of Moynihan et al. (1976) where

$$\left.\frac{dT_f}{dT}\right|_T = \frac{\left[C_p(T) - C_{pg}(T)\right]\big|_T}{\left[C_{pe}(T) - C_{pg}(T)\right]\big|_{T_f}} \tag{5}$$

(Narayanaswamy 1971; Moynihan et al. 1976) where the molar heat capacity C_p (J mol^{-1} K^{-1}) = molar mass (g mol^{-1}) x c_p (J g^{-1} K^{-1}). Equation 5 can be rewritten as

$$\int_{T'}^{T^*} \left[C_p(T) - C_{pg}(T)\right]dT = \int_{T_f'}^{T^*} \left[C_{pe}(T) - C_{pg}(T)\right]dT_f \tag{6}$$

based upon the relationship between the temperature-dependent heat capacity and the temperature-dependent fictive temperature (DeBolt et al. 1976) for T_f fictive temperature, T temperature in K, C_p heat capacity as a function of temperature, C_{pg} unrelaxed (glassy) heat capacity as a function of temperature, C_{pe} relaxed heat capacity as a function of temperature; with T_f' limiting fictive temperature and T^* a temperature above the glass transition region at which the heat capacity is equal to the equilibrium heat capacity (fictive temperature is equal to furnace temperature), T' a temperature below the glass transition region at which the heat capacity is that of the unrelaxed glass. Equation 6 is shown graphically in Fig. 3 where the integral is illustrated in terms of the area under the heat capacity curve.

Results and discussion

The viscosity of the melts is listed as a function of temperature in Table 3 and shown in Figs. 4 and 5 as a function of inverse temperature. The Arrhenian equation

$$\eta = \eta_0 \, exp^{\frac{E}{RT}} \tag{7}$$

for η_0 the viscosity constant in Pa s and E the activation energy for flow in kJ mol^{-1}, T temperature in K and the gas constant $R = 8.314$ J mol^{-1} K^{-1} is fit to the data in the form

$$log_{10} \, \eta = A_{Arr} + \frac{B_{Arr}}{ln \, (10) \, RT} \tag{8}$$

for A_{Arr} a constant = $log_{10} \eta_0$, B_{Arr} activation energy in kJ mol^{-1}. The parameters to the fit are given in Table 4.
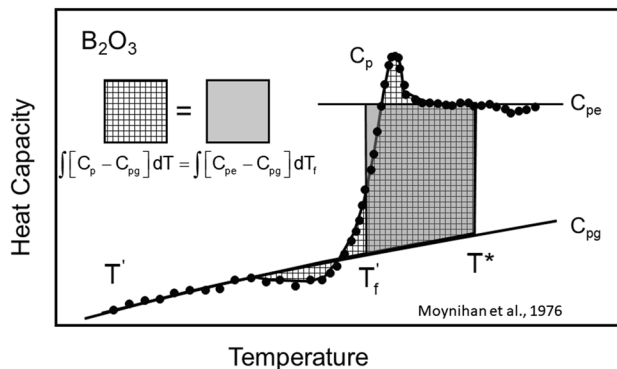

Fig. 3 Graphical representation of Eq. 6, as found in Moynihan et al. (1976), showing the two integrals which need to equal to each other in order to determine the limiting fictive temperature T'_f

Table 3 $\log_{10}$ viscosity for the different GHM melts

T (°C)	$\log_{10}\eta$ (Pa s)	T (°C)	$\log_{10}\eta$ (Pa s)	T (°C)	$\log_{10}\eta$ (Pa s)	T (°C)	$\log_{10}\eta$ (Pa s)
a20		22b				34	
711.3	13.44	710.2	13.05	12a		830.7	11.19
721.7	13.27	730.0	12.30	812.0	11.63	831.5	10.96
730.0	13.13	750.3	11.94	832.3	11.43	850.5	10.87
750.3	12.73	769.8	11.45	852.0	11.09	850.8	10.78
790.7	11.86	790.7	10.94	10		870.6	10.43
811.1	11.45	810.4	10.43	691.0	11.91	870.7	10.31
830.3	11.11	829.9	10.05	711.1	11.36	890.7	9.99
841.3	10.99	848.3	9.72	711.3	11.25	891.1	9.96
850.6	10.76	868.4	9.52	711.9	11.34	910.1	10.08
870.4	10.46	888.7	9.29	731.3	10.65	910.8	9.59
890.7	10.12	928.3	8.65	731.4	10.83	929.5	9.51
890.7	10.11	5a		7		930.4	9.62
909.1	9.87	713.2	12.47	731.4	13.55	950.4	9.10
909.9	9.84	734.0	11.87	752.7	13.29	950.6	9.13
939.2	9.21	752.8	11.38	772.5	12.68	16b	
949.4	9.13	732.0	11.90	792.9	12.29	810.4	11.49
a19		751.7	11.47	812.9	11.88	828.8	11.15
830.8	10.88	h22b		832.6	11.56	848.2	10.68
850.0	10.51	709.3	13.17	852.7	11.15	869.2	10.38
869.5	10.17	729.1	12.50	872.8	10.82	889.5	9.92
888.8	9.95	748.5	11.98	892.4	10.32	908.8	9.63
908.5	9.52	768.9	11.33	912.1	10.12	928.4	9.24
949.2	8.92	787.8	10.69	932.1	9.74	948.4	8.89
h16b		807.7	10.27	h12a		h5a	
768.4	12.30			687.5	12.71	668.0	13.43
787.9	11.75			707.5	11.90	688.4	12.67
808.0	11.32			727.5	11.11	708.3	11.89
827.1	10.91			747.7	10.25	728.4	11.32
846.3	10.46			767.2	9.70	748.3	10.68
866.7	10.02			786.4	9.00	767.7	10.11

Table 3 (continued)

T °C	$\log_{10}\eta$ Pa s	T °C	$\log_{10}\eta$ Pa s	T °C	$\log_{10}\eta$ Pa s	T °C	$\log_{10}\eta$ Pa s
885.2	9.71	827.0	9.77	806.4	8.39	787.8	9.58
904.5	9.37	846.3	9.21	825.7	7.91	827.8	8.85
h34		866.4	9.15	NIQ		h10	
707.4	12.15	885.4	8.68	662.2	10.98	687.1	13.12
727.3	11.20	904.9	8.32	682.5	9.99	786.3	9.15
748.8	10.38	924.8	8.14	703.0	9.29	806.6	8.58
766.5	9.73			722.7	8.64	826.1	7.88
766.5	9.78			742.9	7.78		
786.3	9.13						
806.8	8.51						

X-ray diffraction of the iron-bearing samples indicates a minor amount of crystallization (< 3 vol%) has taken place during the viscosity and calorimetry measurements. A check on the extent of the effect of crystallization on viscosity was made plotting T_g^{12} (the temperature at which $\eta = 10^{12}$ Pa s) against γ. Previous studies have shown that a smooth curve as a function of gamma is to be expected in a series of compositionally related melts, with T_g^{12} increasing as the melts becomes subaluminous. Figure 6 illustrates the T_g^{12} values determined from the viscosity data for both the iron-bearing and iron-free melts. It can be seen that the data points for the Mt. Mee (34) and Maleny (12a) composition melts are much higher than expected, thus indicating that the melts had a large volume of crystals and the viscosity data are not that of a crystal-free melt. The Einstein-Roscoe equation (e.g. Vetere et al. 2013) for the viscosity of crystal-bearing melts indicates that 40 vol% crystals are needed to increase viscosity by an order of magnitude. In the case of the Mt. Mee and Maleny samples, it is observed that the interior of the glasses contained < 3 vol% micro-crystals, and the surface of the samples was covered with a thin veneer of micro-crystals after the viscosity measurements. As the micro-penetration technique measures the viscosity of the first ~ 500 μm of the sample, it would appear that the large number of crystals seen on the surface of the samples affects the measured viscosity of these two samples.

The temperature at which viscosity is 10^{12} Pa s has been calculated from the Arrhenian fits to the viscosity data and listed in Table 4. These T_g^{12} values have also been added to the composition data of Fig. 2. The importance of network modifiers is illustrated by the three SiO_2-rich samples which have T_g^{12} values that do not linearly vary with wt% SiO_2. The T_g^{12} values do vary linearly if they are plotted as a function of γ – which is a measure of the non-bridging oxygens in the melt. These three melts range from metaluminous (γ > 0.5), to subaluminous (γ = 0.5) to peraluminous (γ < 0.5).

The Arrhenian equation should not be extrapolated linearly in temperature. Instead the configurational heat capacity and the Adam-Gibbs equation (Richet 1984) have been used to fit the viscosity data across of the entire temperature range:

$$log_{10}\eta = A_{AG} + \frac{B_{AG}}{ln(10)\left\{ T \cdot \left[S_{conf}\left(T_g^{12}\right) + C_p^{conf} \cdot ln\left(\frac{T}{T_g^{12}}\right) \right] \right\}} \quad (9)$$

in order to calculate the temperature dependence of the viscosity at high temperatures; for A_{AG} a constant, taken to be − 4.55 (see Giordano et al. 2008; Kleest et al. 2020 and references therein); B_{AG} activation energy (J mol^{-1}), $S_{conf}(T_g^{12})$ configuration entropy (J mol^{-1} K^{-1}) at the temperature for which viscosity is 10^{12} Pa s, C_p^{conf} the difference in

Fig. 4 Viscosity of the Glass House Mountains melts as a function of inverse temperature. The data for melts 34, 16b, 12a and a19 are shifted to the right on the X-axis by the amount given in brackets for clarity. The straight lines are Arrhenian fits to the data
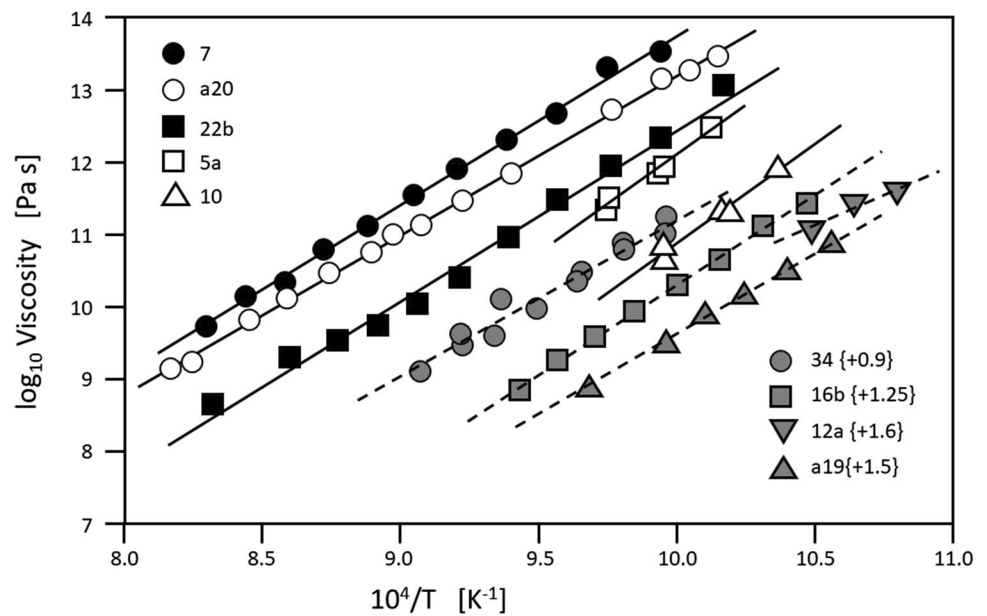
Fig. 5 Viscosity of the iron-free haplo-Glass House Mountains melts and the NIQ melt as a function of inverse temperature. The data for melts H34 and H10 are shifted to the right on the X-axis by the amount given in brackets for clarity. The straight lines are Arrhenian fits to the data. The curve through the NIQ data is that of Whittington et al. (2000)
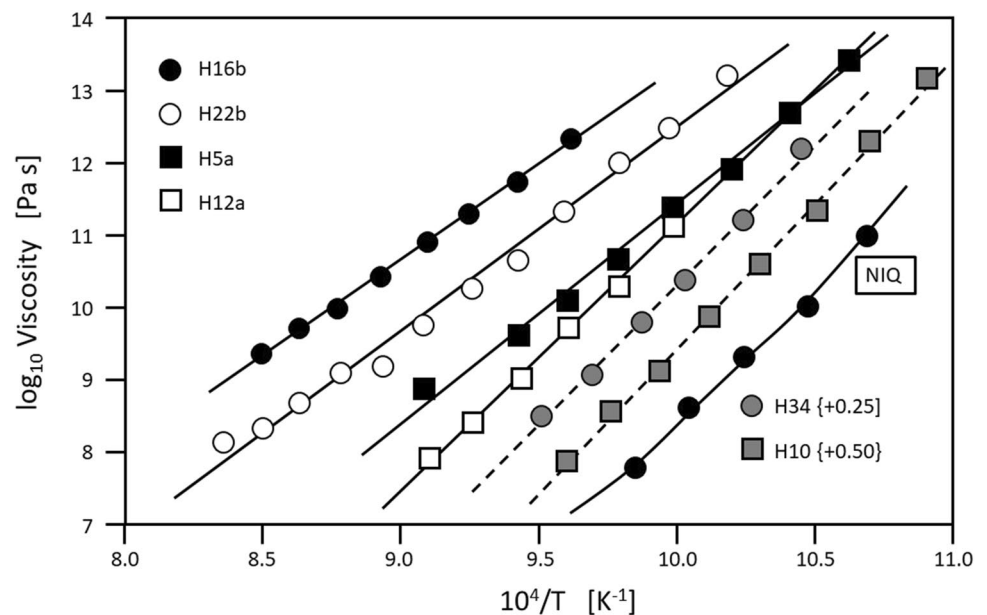
extrapolated glass heat capacity and relaxed melt heat capacity (J mol^{-1} K^{-1}) at a temperature above the glass transition. This equation describes the viscosity-temperature behaviour of the melt from the temperature range of measurement to higher temperatures. The parameters B_{AG} and $S_{conf}(T_g^{12})$ are listed in Table 4.

This equation assumes there is no change in $S_{conf}(T_g^{12})$ nor in C_p^{conf} for temperatures below T_g^{12}. The value for the parameter A is assumed to be constant for all silicate melts and thus independent of composition (Toplis et al. 1997). Based on the Maxwell relation (Eq. 2) and taking $\tau_0 = 10^{-14.5}$ s (the vibration frequency of an atom at $T^{-1} = 0$; Martinez and Angell (2001)) and $G_\infty = 10 \pm 0.5$

GPa (Dingwell and Webb 1989), the $A_e = -4.55$ log$_{10}$ Pa s is used in this study. The same value was used in the model of Giordano et al. (2008). The values of A found in the literature range from -2.6 (Toplis 1998) to -5 (see Webb 2011; Russell and Giordano 2017 for a discussion). Russell and Giordano (2017) point out that $-5 < A < -3$ is found to be the range of values used for the constant A in the literature; with $-4 < A_{AG} < -3$ for Adam-Gibbs fits to viscosity data and $-5 < A_{VFT} < -4$ for Vogel-Fulcher-Tammann equation fits to the viscosity data. They found the best fit value for A_{AG} to be -3.51 ± 0.25. The $S_{conf}(T_g^{12})$ values obtained from the present viscosity and C_p^{conf} data

Table 4 Measured properties (γ, T_f^{20}, T_g^{12}, c_p^{glass}, c_p^{melt}, C_p^{conf}) determined from the composition and the heat capacity and the viscosity data together with the fit parameters to the viscosity data using the Arrhenian equation (A_{Arr}, B_{Arr}) and the fit parameters for viscosity data using the Adam-Gibbs equation ($S^{conf}(T_g^{12})$, B_{AG}) for the iron-bearing melts and iron-free melts. Fragility m is calculated from an Arrhenian fit to the viscosity data m_{Arr} and the Adam-Gibbs fit to the viscosity data m_{AG}

	γ	T_f^{20} K	T_g^{12} K	c_p^{glass} J g^{-1} K^{-1}	c_p^{melt} J g^{-1} K^{-1}	C_p^{conf} J mol^{-1} K^{-1}	m_{Arr}	A_{Arr} log$_{10}$ (Pa s)	B_{Arr} kJ mol^{-1}	$A_{AG}=-4.55$ m_{AG}	$S^{conf}(T_g^{12})$ J mol^{-1} K^{-1}	B_{AG} kJ mol^{-1}	$A_{AG}=-3.51$ m_{AG}	$S^{conf}(T_g^{12})$ J mol^{-1} K^{-1}	B_{AG} kJ mol^{-1}
20a	0.50	1050.3	1056.5	1.14	1.22	5.21	20.7	-8.71 ±0.20	419.0 ±4.3	21.2	19.58 ±1.11	798.6 ±45.2	20.9	14.81 ±0.72	558.05 ±26.70
19a	0.52	1026.5	1045.5	1.12	1.18	4.28	21.2	-9.24 ±0.56	424.8 ±12.4	22.2	12.76 ±1.65	509.7 ±63.4	22.5	9.59 ±1.04	359.40 ±37.10
16b	0.50	1045.0	1060.7	1.11	1.19	5.41	23.5	-11.47 ±0.35	476.7 ±7.7	24.9	11.01 ±0.68	449.8 ±25.5	25.0	8.9 ±0.47	337.95 ±17.22
22b	0.54	1019.5	1018.4	1.10	1.24	9.15	23.2	-11.14 ±0.75	451.4 ±15.4	24.3	19.95 ±2.00	779.7 ±75.0	24.3	16.09 ±1.33	585.15 ±47.14
5a	0.60	1010.0	1002.8	1.10	1.23	8.33	26.7	-14.69 ±1.19	512.4 ±23.1	26.9	13.41 ±1.58	513.1 ±57.6	26.8	11.41 ±1.16	408.35 ±41.20
34	0.68	1145.0	1055.5	1.07	1.16	6.50	20.6	-8.58 ±1.07	415.8 ±23.8	21.2	23.05 ±6.40	928.8 ±248.4	21.5	16.87 ±3.73	637.29 ±135.56
12a	0.68	987.0	1061.0	1.09	1.34	16.27	15.5	-3.48 ±2.51	314.4 ±43.2	-	-	-	-	-	-
10	0.71	975.3	961.3	1.00	1.19	12.52	29.3	-17.27 ±2.26	538.7 ±42.8	30.1	15.29 ±2.81	560.3 ±100.7	30.4	13.117 ±2.25	452.22 ±75.2
7	0.49	1107.0	1080.8	1.13	1.21	5.58	21.7	-9.68 ±0.38	448.4 ±7.9	21.8	17.61 ±1.40	724.5 ±57.1	21.8	13.69 ±0.93	527.51 ±35.55
h20a	0.53	1066.5	-	1.50	1.55	3.42	-	-	-	-	-	-	-	-	-
h19a	0.53	1085.0	-	1.72	1.93	13.06	-	-	-	-	-	-	-	-	-
h16b	0.51	1061.4	1052.0	1.53	1.67	9.21	25.0	-13.07 ±0.34	504.7 ±7.2	26.0	16.1 ±0.52	643.9 ±20.2	26.2	13.27 ±0.37	497.88 ±13.4
h22b	0.55	1024.0	1017.6	1.15	1.32	11.20	27.5	-15.48 ±0.81	535.2 ±16.8	29.3	14.4 ±0.84	556.8 ±31.4	29.9	12.09 ±0.64	439.66 ±21.36
h5a	0.61	992.0	985.6	1.60	1.85	16.56	30.8	-28.18 ±0.95	757.6 ±18.5	32.1	17.3 ±0.76	644.0 ±27.4	32.2	15.03 ±0.56	522.52 ±19.16
h34	0.68	992.0	982.6	1.53	1.92	24.39	38.9	-27.11 ±1.02	735.8 ±20.1	43.3	14.9 ±0.33	553.8 ±24.4	44.5	13.04 ±0.26	457.83 ±7.96
h12a	0.68	986.3	977.1	1.51	1.94	27.63	37.9	-25.91 ±0.61	757.6 ±12.1	42.2	17.8 ±0.38	662.0 ±27.6	43.0	15.63 ±0.36	545.85 ±11.71
h10	0.70	998.0	985.5	1.49	1.93	27.64	40.1	-28.25 ±0.53	757.4 ±10.5	43.8	16.6 ±0.36	619.2 ±27.6	44.3	14.75 ±0.47	516.02 ±15.46
h7	0.49	1123.0	-	1.53	1.66	8.21	-	-	-	-	-	-	-	-	-
NIQ	0.89	918.3	912.3	1.18	1.65	28.31	41.6	-29.56 ±1.39	725.9 ±25.3	46.9	15.5 ±0.75	540.9 ±24.4	49.8	12.97 ±0.89	426.49 ±25.88

Some melts crystallised during the viscosity measurements, and therefore, there is no data available
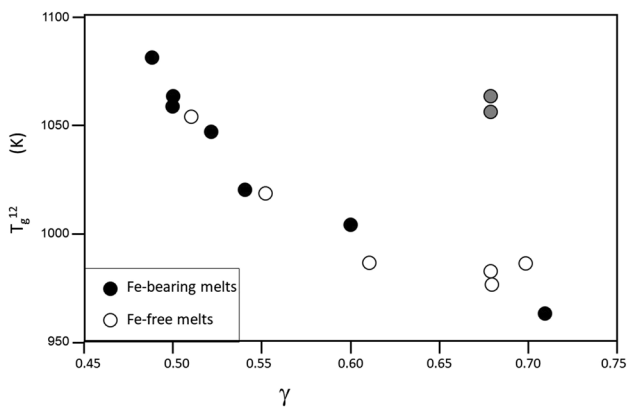
Fig. 6 T_g^{12} determined from the viscosity measurements as a function of composition. The data points for the Mt. Mee (34) and Maleny (12a) composition melts are shaded grey
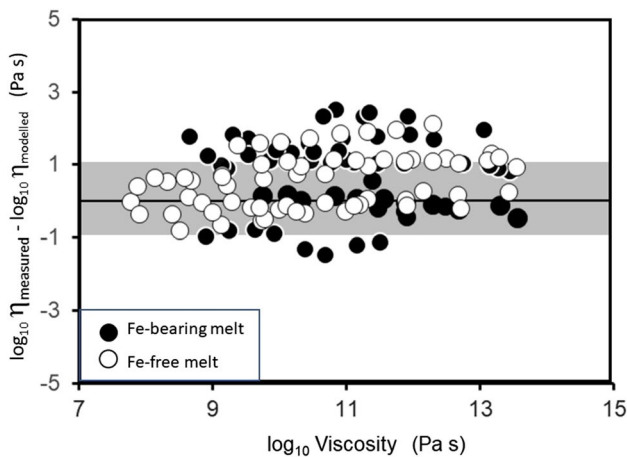

Fig. 7 Misfit between modelled viscosity of Giordano et al. (2008) and the measured viscosities as a function of measured viscosity

using this value of A_{AG} are also given in Table 4. The fragility of the melts was also calculated from:

$$m = \left.\frac{d\log_{10}\eta}{d\left(T_g^{12}/T\right)}\right|_{T=T_g^{12}} = \frac{B_{Arr}}{\ln(10)RT_g^{12}} = \frac{B_{AG}}{\ln(10)S_{conf}\left(T_g^{12}\right)\cdot T_g^{12}}\left[1+\frac{C_p^{conf}\left(T_g^{12}\right)}{S_{conf}\left(T_g^{12}\right)}\right] \tag{10}$$

(Toplis et al. (1997)

The viscosity prediction models of Hui and Zhang (2007) and Giordano et al. (2008) in which it is assumed that the Fe^{2+}/Fe_{tot} is constant for all melts investigated, and Duan (2014) which differentiates between Fe^{2+} and Fe^{3+}, have been compared to the present viscosity data. These models estimate the viscosity of the iron-bearing and iron-free melts to within ± 2 orders of magnitude. The difference between the measured viscosity of the present melts and that predicted by the Giordano et al. (2008) model is shown in Fig. 7.
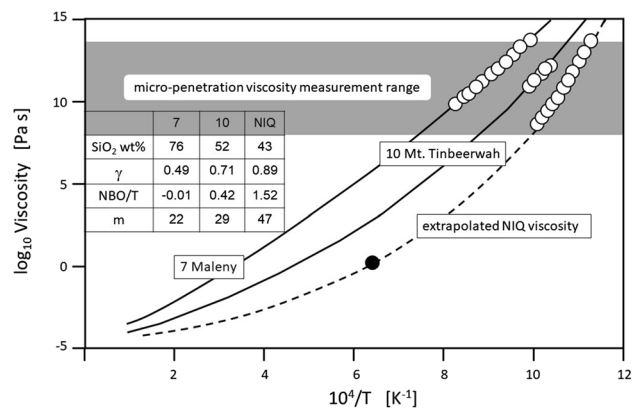
Fig. 8 Extrapolation of the measured viscosity data for the Glass House Mountains magmas. The viscosity is extrapolated using the Adam-Gibbs equation and the present heat capacity data (see Table 4). The two viscosity curves are for the least and most fragile (m) of the melts and also for the highest and lowest melt viscosities of the system. The viscosity data for the NIQ melt are also shown

The variation of C_p^{conf} and $S_{conf}(T_g^{12})$ as a function of γ, and also SiO_2 content can be observed in Table 4. While $S_{conf}(T_g^{12})$ does not show any clear trend as a function of composition, the C_p^{conf} values increase with decreasing polymerisation of the melts. Giordano and Russell (2017) found the measured C_p^{conf} values for a series of silicate melts to be a linear function of mole fraction SiO_2 with $C_p^{conf} = 52.6 - 55.88\,X_{SiO_2}$. The present C_p^{conf} data for both the iron-bearing and iron-free melts scatter around this trend-line with $C_p^{conf}(GHM) = 50.35 - 54.43\,X_{SiO_2}$.

Russell and Giordano (2017) found the ratio of the measured C_p^{conf} to the fitted S_{conf} value to be a function of T_g^{12} and fragility (m). The C_p^{conf} and S_{conf} determined here from heat capacity and viscosity measures and calculated with $A_{AG} = -4.55$ fall slightly off this trendline ($C_p^{conf}/S_{conf}(T_g^{12}) = 0.061\ m - 1.018$). However, the ratio obtained using the S_{conf} values determined from the viscosity data assuming an A_{AG} of -3.51 fall exactly on the trendline of Russell and Giordano (2017) (0.064 m – 0.993). The T_g^{12} term has been ignored here in these straight-line fits to the data as its contribution to the equation of Russel and Giordano is ~ 0.004.

Figure 8 shows the viscosity of melts 7 (Maleny) and 12 (Mt. Tinbeerwah) calculated from Eq. 9 together with the viscosity region of the input data. This figure also shows the present viscosity data for the NIQ sample, together with the high temperature datum from Whittington et al. (2000) and the curves calculated by Whittington et al. and the present Adam-Gibbs curve. The two curves are identical (within 0.1 $\log_{10}$ unit); and both pass though the datum of Whittington et al. (2000). This agreement between the viscosity extrapolated using the Adam-Gibbs equation and the measured low viscosity indicates the applicability of the Adam-Gibbs

Table 5 Calculated discharge rate for a cylindrical vent with estimated eruption temperatures, rock and melt densities and viscosities of the present Glass House Mountains melts

Volcano	10	5a	16b	20a
	Basalt	Andesite	Dacite	Rhyolite
Temperature °C	1250	1075	1075	900
Rock density kg m^{-3}	3300	3300	3300	3300
Melt density kg m^{-3}	2650	2510	2392	2350
Vent radius m	2.5	2.5	2.5	2.5
Viscosity log$_{10}$ Pa s	1.20	5.16	7.00	9.95
Magma volume km^3 day^{-1}	0.53	7.1×10^{-5}	1.2×10^{-6}	1.4×10^{-9}

equation in the calculation of low viscosities, based on the high viscosity data combined with the configuration heat capacity.

As there is little or no information on the eruption temperature of the lavas of the Glass House Mountains volcanoes, it is difficult to estimate the amount of magma involved. Further, although the mafic lavas near Maleny are present, the lavas and/or pyroclastics of the rest of the Glass House Mountains volcanoes appear to have been removed by erosion (Ewart & Grenfell 1985; Cohen et al. 2007).

Taking the best-case scenario to calculate the discharge rate of a volcanic conduit, the volume flow rate of a frictionless cylindrical volcanic conduit can be calculated from:

$$V = \frac{\pi g (\rho_r - \rho_m) r^4}{8\eta} m^3 s^{-1} \qquad (11)$$

for acceleration due to gravity 9.81 m s^{-2}, rock density ρ_r (kg m^{-3}), melt density ρ_m (kg m^{-3}), radius of the vent r (m) and viscosity of the melt η (Pa s) (Philpotts 1990). The rate of flow through such a conduit calculated using the average eruption temperature of each composition melt (taken from Spera 2000), the viscosity of the present melt at that temperature, and the density of the present melt calculated from Lange and Carmichael (1987) and the assumption that the source of the magma is the upper mantle with a density of 3300 kg m^{-3}, is shown in Table 5. The mafic lavas around Maleny are known to cover 200 km^2, and to be made up of ~ 10 m thick layers to a total depth of 180 m (Ewart and Grenfell 1985; Cohen et al. 2007). The calculations of Table 5 would indicate that 68 days of continuous eruption with a 2.5-m radius vent are needed to produce 36 km^3 of basaltic lava, with 4 days eruption time needed to cover the surface with a 10-m-thick layer. These calculations would infer that the basaltic eruptions were of short duration, or that the vent radius was smaller than 2.5 m. A reduction of

the radius by 15% would halve the flow rate. Doubling the radius of the vent would increase the volume flow rate by more than an order of magnitude.

Conclusion

The combination of low temperature viscosity data with low temperature heat capacity data allows the use of the Adams-Gibbs equation to extrapolate the viscosity of the Glass House Mountains magma to higher temperature with great confidence. Based on the small basalt flows observed in the Maleny region it is suggested that the discharge rate of the more viscous melts would be very low and perhaps, as suggested by Ewart and Grenfell (1985) and Cohen et al. (2007) the Glass House Mountains are the remnants of unextruded magmas which formed plugs and laccoliths. The effect of water and perhaps bubbles would, however, decrease the viscosity. Stevenson et al. (1998) found that 1 wt% water decreased the viscosity of comendites by 2 or more orders of magnitude in the temperature range of interest. This would increase the discharge rate by 2 orders of magnitude. In the case of the comendite compositions (as well as the dacite and andesite) such an increased discharge rate would still remain very low when compared to that of the basalt melts.

References

Bryan WB, Stevens NC (1973) Holo-crystalline pantellerite from Mt. Ngun-Ngun, Glass House Mountains, Queensland. Australia Am J Sci 273:947–957

Cohen BE, Knesel KM, Vasconcelos PM, Schellart WP (2013) Tracking the Australian plate motion through the Cenozoic: contraints from ^{40}Ar/^{39}Ar geochronology. Tectonics 32:1371–1383

Cohen BE, Vasconcelos PM, Knesel KM (2007) $^{40}Ar/^{39}Ar$ constraints on the timing of Oligocene intraplate volcanism in southeast Queensland, Australia. Aust J Earth Sci 54:1205–2125

Davies DR, Rawlinson N, Campbell ICH (2015) Lithospheric controls on magma composition along Earth's longest continental hotspot track. Nature 525:511–514

DeBolt MA, Easteal AJ, Macedo PB, Moynihan CT (1976) Analysis of structural relaxation in glass using rate heating data. J Am Ceram Soc 59:16–21

Di Genova D, Romano C, Hess KU, Vona A, Poe PT, Giordano D, Dingwell DB, Behrens H (2013) The rheology of peralkaline rhyolites from Pantelleria Island. J Volc Geotherm Res 249:201–216

Dingwell DB, Knoche R, Webb SL (1992) The effect of B_2O_3 on the viscosity of haplogranitic liquids. Am Mineral 77:457–461

Dingwell DB, Webb SL (1989) Structural relaxation in silicate melts and non-Newtonian Melt rheology in geological processes. Phys Chem Minerals 16:508–516

Duan X (2014) A model for calculating the viscosity of natural iron-bearing silicate melts over a wide range of temperatures, pressure, oxygen fugacites, and compositions. Am Mineral 99:2378–2388

Ewart A, Grenfell AT (1985) Cainozoic volcanic centres in south-eastern Queensland: with special reference to the Main Range, Bunya Mountains, and the volcanic centres of the northern Brisbane coastal region. Papers, Department of Geology, University of Queensland, 11:1–57

Giordano D, Russell JK (2017) The heat capacity of hydrous multi-component natural melts and glasses. Chem Geol 461:96–103

Giordano D, Russell JK, Dingwell DB (2008) Viscosity of magmatic liquids: a model. EPSL 271:123–134

Herzfeld TA, Litovitz KF (1959) Absorption and dispersion of ultra-sonic waves. pp 535, Academic Press, New York

Hui H, Zhang Y (2007) Toward a general viscosity equation for natural anhydrous and hydrous silicate melts. Geochim Cosmochim Acta 71:403–416

Kleest C, Webb SL, Fanara S (2020) Rheology of melts from the Colli Albani volcanic district (Italy): a case study. Contrib Mineral Petrol 175:82

Lange RA, Carmichael ISE (1987) Densities of Na_2O-K_2O-CaO-MgO-FeO-Fe_2O_3-Al_2O_3-TiO_2-SiO_2 liquids – new measurements and derived partial molar properties. Geochim Cosmochim Acta 51:2931–2946

Maier CG, Kelley KK (1932) An equation for the representation of high-temperature heat content data. J Am Chem Soc 54:3243–3246

Martinez LM, Angell CA (2001) A thermodynamic connection to the fragility of glass-forming liquids. Nature 410:663–667

Maxwell JC (1867) On the dynamical theory of gases. Proc Roy SocLondon 15:167–171

Misiti V, Vetere F, Freda C, Scarlato P, Behrens H, Mangiacapra A, Dingwell DB (2011) A general viscosity model of Campi Flegrei (Italy) melts. Chem Geol 290:50–59

Moynihan CT, Easteal AJ, DeBolt MA, Tucker J (1976) Dependence of fictive temperature of glass on cooling rate. J Am Ceram Soc 59:12–16

Narayanaswamy OS (1971) Model of structural relaxation in glass. J Am Ceram Soc 54:491–498

Philpotts AR (1990) Principles of Igneous and Metamorphic Petrology. Prentice Hall

Pocklington HC (1940) Rough measurement of high viscosities. Proc Cambridge Phil Soc 36:507–508

Richet P (1984) Viscosity and configurational entropy of silicate melts. Geochim Cosmochim Acta 48:471–483

Robert G, Knipping JL, Scherbarth S, Robertson TE, Stechern A, Behrens H, Whittington AG (2015) Heat capacity and viscosity of basaltic melts with $H_2O \pm F \pm CO_2$. Chem Geol 418:51–65

Robie RA, Hemingway BS, Fischer JR (1978) Thermodynamic properties of minerals and related substances at 29815 K and 1 bar (105 Pa) pressure and at higher temperatures. US Geolog Surv Bull 1452:428–446

Russell JK, Giordano D (2017) Modelling configurational entropy of silicate melts. Chem Geol 461:140–151

Schuessler JA, Botcharnikov RE, Behrens H, Misiti V, Freda C (2008) Oxidation state of iron in hydrous phono-tephritic melts. Am Mineral 93:1493–1504

Sehlke A, Whittington AG (2016) The viscosity of planetary tholeiitic melts: a configurational entropy model. Geochim Cosmochim Acta 191:277–299

Shannon RD, Prewitt CT (1969) Effective ionic radii in oxides and fluorides. Acta Cryst B25:925–946

Shao F, Nui Y, Regelous M, Zhu DC (2015) Petrogenesis of peralkaline rhyolites in an intra-plate setting: Glass House Mountains, southeast Queensland, Australia. Lithos 216:196–210

Spera F (2000) Physical Properties of magma. In: Sigurdsson H (ed) Encyclopedia of Volcanoes. Academic Press, Amsterdam, pp 171–190

Stevenson RJ, Dingwell DB, Webb SL, Bagdassarov NS (1995) The equivalence of enthalpy and shear stress relaxation in rhyolitic obsidians and quantification of the liquid-glass transition in volcanic processes. J Volc Geotherm Res 68:297–306

Stevenson RJ, Bagdassarov NS, Dingwell DB, Romano C (1998) The influence of trace amounts of water on the viscosity of rhyolites. Bull Volcanol 60:89–97

Toplis MJ (1998) Energy barriers to viscous flow and the prediction of glass transition temperatures of molten silicates. Am Mineral 83:480–490

Toplis MJ, Dingwell DB, Hess KU, Lenci T (1997) Viscosity, fragility, and configurational entropy of melts along the join SiO_2-$NaAlSiO_4$. Am Mineral 82:979–990

Vetere F, Behrens H, Schuessler JA, Holtz F, Misiti V, Borchers L (2008) Viscosity of andesite melts and its implication for magma mixing prior to Unzen 1991–1995 eruption. J Volc Geotherm Res 172:208–217

Vetere F, Sato H, Ishebashi H, De Rosa R, Donato P (2013) Viscosity changes during crystallization of a shoshonitic magma: new insights on lava flow emplacement. J Min Petrol Sci 108:144–160

Webb S (2005) Structure and rheology of iron-bearing Na_2O-Al_2O_3-SiO_2 melts. Europ J Mineral 17:223–232

Webb SL (1991) Shear and volume relaxation in $Na_2Si_2O_5$. Am Mineral 9:1449–1454

Webb SL (2008) Configurational heat capacity of Na_2O-CaO-Al_2O_3-SiO_2 melts. Chem Geol 256:92–101

Webb SL, Murton BJ, Wheeler AJ (2014) Rheology and the Fe^{3+}-chlorine reaction in basaltic melts. Chem Geol 366:24–31

Webb SL (2011) Configurational heat capacity and viscosity of (Mg, Ca, Sr, Ba)O-Al_2O_3-SiO_2 melts. Europ J Mineral 23:487–497

Whittington A, Richet P, Holtz F (2000) Water and the viscosity of depolymerized aluminosilicate melts. Geochim Cosmochim Acta 64:3725–3736

Whittington AG, Hellwig BM, Behrens H, Joachim B, Stechern A, Vetere F (2009) The viscosity of hydrous dacitic liquids: implications for the rheology of evolving silic magmas. Bull 71:185–199

Wilson AD (1969) The micro-determination of ferrous iron in silicate minerals by a volumetric and a colorimetric method. Analyst 85:823